Postprint of: Grabski M., Ambroziak A., Experimental and analytical analysis of punching shear in flat slabs supported on column topped with concrete head, CONSTRUCTION AND BUILDING MATERIALS Vol. 364 (2023), 129961, DOI: 10.1016/j.conbuildmat.2022.129961

EXPERIMENTAL AND ANALYTICAL ANALYSIS OF PUNCHING SHEAR IN FLAT SLABS SUPPORTED ON COLUMN TOPPED WITH CONCRETE HEAD

Maciej Grabski[1,2] & Andrzej Ambroziak[1] *)

[1] Gdańsk University of Technology, Faculty of Civil and Environmental Engineering, St. Gabriela Narutowicza 11/12, 80-233 Gdansk, Poland, ambrozan@pg.edu.pl

[2] Maciej Grabski Engineering, 94B/1 Leszczynowa Street, 80-175 Gdańsk; grabski@gengineering.pl

Abstract: An experimental laboratory test of the two series of slab-column elements topped with drop panels of varying sizes is described in this paper. The scope of the paper is to investigate the influence of the drop panel size and stiffness on the behaviour of the connection between the flat slab and the column topped by the concrete head. The impact of the head size and stiffness is analysed analytically and experimentally. The experimental test results show that at a ratio $h_{sh}/l_{sh} \leq 0.55$ the heads are too flexible to cause punching shear outside the head, confirm significant concentrations of shear forces at the corners of the large support, and show a significant contribution of the linear parts of the control perimeter to the ultimate force transmitted by the slab-column joint. The authors compare the experimental test results with the considered standard calculation methods and indicate the correlations. The paper provides new experimental results and proposals for the application of a reduction factor for permissible shear stresses in the EC2 standard that depends on the dimension of the support. Simultaneously, the experimental results and the comparison with the standard calculations indicate a further need for research on the connection of a slab to a column topped by a drop panel.

Keywords: reinforced concrete; slab-column connections; punching shear; drop panel; shear cap

1. Introduction.

Slab-column structures nowadays represent a large part of the building construction industry. Flat slabs provide the possibility of easily changing the arrangement and use of usable space in the building. In the case of tall buildings, they can also reduce the height of the storey, which leads to more efficient use of free space. All these features make flat slab structures a permanent subject of a lot of experimental research [1–8]. One of the key issues in the design of slab-column structures is the phenomenon of slab shear punching caused by stress concentrations in the slab near the point support [9,10]. Many parameters that influence punching shear resistance are investigated and described, e.g. support shape and dimension [11–13], type and strength of concrete [14–18], the effect of the hole near support [19,20], membrane effect [21,22], cyclic load [23,24]. The investigations of a structure after its failure as a result of punching [25–28] or strengthening against punching shear [17,29] are also performed. One way to increase the punching shear resistance of the slab-column joint is to provide additional shear reinforcement in the form of stirrups and transverse reinforcement [30–34], double-headed studs [35], rigid steel profiles [36,37], UHPFRC hidden capitals [38,39] in the vicinity of the connection. Another way to increase the load bearing capacity of a slab-column joint is to extend the column in the vicinity of the slab (column capital) or to thicken the slab in the area of the point support at the support

(drop panel) [40,41]. This type of enhancement is widely used today because it increases the punching shear resistance of the slab-column joint while increasing the rigidity of the floor, which has a positive effect on its deformation behaviour.

According to design standards, the design process for the connection of a slab-column with a drop panel requires verification of the punching shear resistance in the head zone and the slab zone outside the head (Fig. 1a). When considering a punching shear situation outside the head zone, the most common cause is that of large flexible support of square or rectangular shapes (Fig.1b).

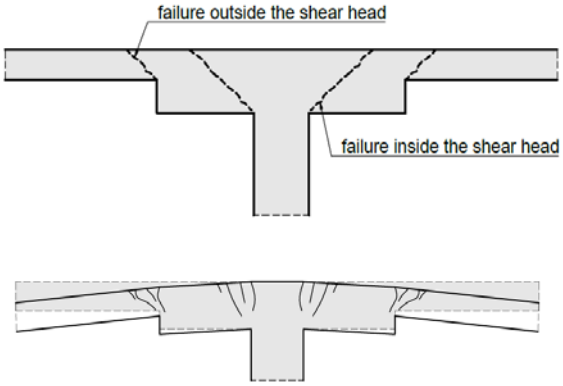

Fig. 1. Column topped with a drop panel: a) potential failure regions; b) drop panel as flexible slab support.

Researchers have revealed, that for large or elongated supports the distribution of shear forces near the support is uneven despite symmetrical loading [42–45] (see Fig. 2). This effect negatively affects the punching shear resistance of the joint [11–13,46–49].

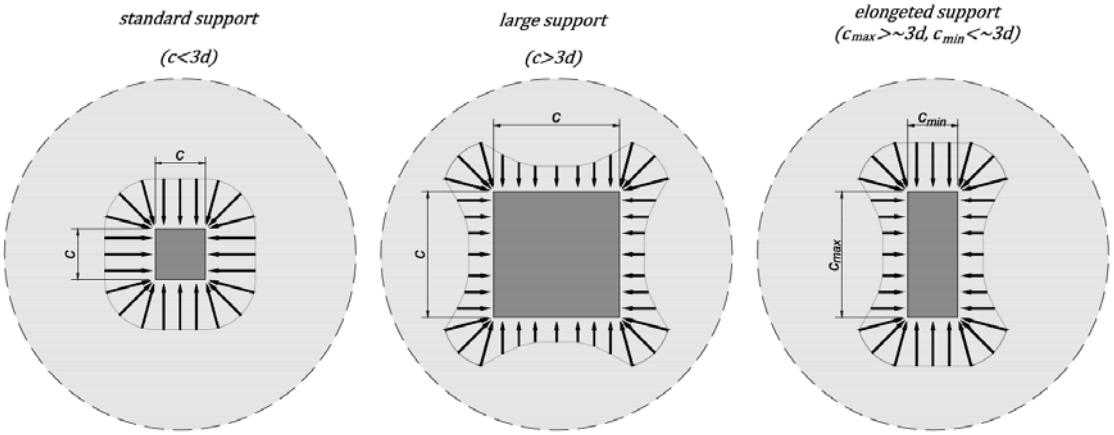

Fig. 2. Distribution of shear forces in the vicinity of internal support as a function of its size and shape.

In most codes, the punching shear strength of the slab-column joint is verified by comparing a nominal shear stress per unit length of the control perimeter to the allowable shear stress of the element, as:

$$v = \frac{V}{b_0 * d} \leq v_R. \tag{1}$$

Therefore, the influence of the load area size on the punching resistance depends on a way to calculate the permitted shear stress (v_R) and the location of the control perimeter (b_0). The different parameters taken into account

to calculate the permissible stresses and the different locations of the control perimeter cause the influence of column size on punching capacity to vary depending on the standard used. In the EC2 standard [50] a non-uniform distribution of the shear forces is accounted for by increasing the acting shear stresses by a factor $\beta > 1.0$ which is a function of the moment transfer between the slab and the column. The EC2 standard doesn't give additional recommendations as to elongated or large load areas. Some European countries have added restrictions on the punching for large supports in national annexes. The EC2-DIN standard [51] imposes a limitation on the length of the control perimeter according to Fig. 3b. Considers this effect by reducing the allowable shear stresses depending on the size and shape of the support. The ACI318 code [52] considers this effect by reducing the allowable shear stresses depending on the size and shape of the support. The first reduction factor is $k_{e,ACI} = \left(2 + \frac{4}{\beta}\right)$, where $\beta = \frac{c_1}{c_2} > 1$, ($c_1, c_2$ – support dimensions; designation $k_{e,ACI}$ is introduced for the purpose of this work). It is decisive for supports with an elongated shape. The second factor is $k_{e,ACI} = \left(2 + \frac{\alpha_s * d}{b_0}\right)$, where α_s - a factor depending on column location. The second factor is decisive for a large support size. The MC2010 standard [53] introduces a simplified method which consists of the control perimeter according to Figure 3c or a general method that explicitly accounts for all effects by length of the control perimeter $b_{0,\text{eff}} = \frac{V}{v_{max}}$ (where $b_{0,\text{eff}}$ is the length of the effective control perimeter, V is the punching force acting on the joint, v_{max} is the maximum value of the shear force per unit length along the perimeter, see Fig. 3d). This formula was proposed by Vaz Rodrigues et al. [54] and it assumed no redistribution of internal forces, which occurs in reality due to the nonlinear behaviour of reinforced concrete (RC) structures [44]. This can be an approximate assumption, especially in the case of large or elongated columns. Setiawan et. al. [55] proposed to replace the value of v_{max} by $v_{3d,av}$:$b_{0,Set} = \frac{V}{v_{3d,av}}$ where $v_{3d,av}$ means the average value of the shear force per unit length occurring in the part of the control perimeter reduced to the corners and straight sections of length 3d, see Fig. 3c.

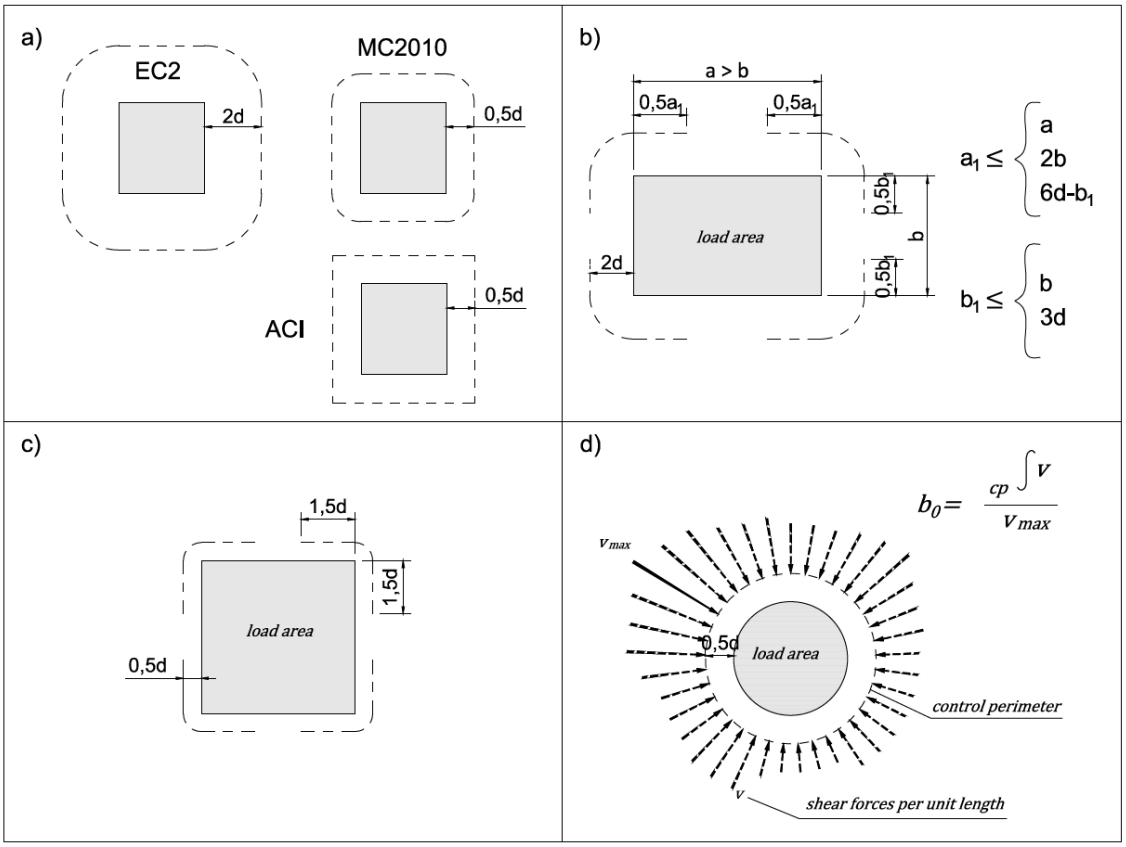

Fig. 3. Control perimeter for punching shear according to different design methods: (a) basic control perimeter of ACI, EC2 and MC2010 standard; (b) Reduction of control perimeter according to EC2-DIN; (c) Reduction of control perimeter according to MC2010-simplified method; (d) Reduction of control perimeter according to MC2010-general method.

The calculation methods used in the standards take into account the effect of non-uniformity of shear forces near the face of the support in different ways. It should be noted that all the standard guidelines have been developed on the basis of tests on flat slabs without drop panels. Computational analyses of the distribution of shear forces in the vicinity of the drop panel show a significant effect of head stiffness and size on the force concentrations at the head corners [45]. It seems advisable to carry out an experimental study of the punching resistance in a situation of drop panel enhancement.

This research presents a unique experimental analysis of punching shear in flat slabs supported on the concrete drop panel. The influence of the drop panel size and stiffness on the behaviour of the connection between the flat slab and the column topped by the drop panel is investigated. The behaviour of the slabs during the test and damage is described. Ultimate loads were compared with the selected calculation methods. The laboratory test results were analysed in terms of allowable shear stresses. Based on the performed experimental tests and analytical analyses, a reduction factor for permissible shear stresses in the EC2 standard that depends on the dimension of the support is proposed. The experimental results and the comparison with the standard calculations indicate a further need for research on the connection of a slab to a column topped by a drop panel.

2. Experimental test description

2.1. General description

The experimental program included two test series of reinforced concrete elements. Six elements were examined during the 1st test series. The first element of the 1st test series was a slab-column element without the drop panel. The other five slab-column elements were with a column topped by drop panels. The only variable for the 1st series of elements was the dimension of the drop panel. The 2nd series of tests contained three elements with drop panels. The dimensions of the concrete head in the elements of the 2nd series corresponded to the dimensions of the drop panels in the three elements of the 1st series, except that they had a lower height of the concrete head. Therefore, the first series of tests conventionally represents rigid drop panels, while the second series of tests represents flexible heads. The elements were tested on a prepared laboratory test stand. On the steel support frame, the slab-column elements were placed as simply supported.The load was imposed vertically by the hydraulic jack, see Figures 4a and 4b.

All slabs were 2000x2000mm in size and 110mm in height. The columns and drop panels of all elements were square. The column dimension for each tested element was 200x200mm. The dimensions of the drop panels in the elements of the 1st series were: 300, 400, 600, 800, and 900 [mm]. The dimensions of the drop panels of the 2nd series elements were: 600, 800, and 900 [mm]. The increased height of the head in the elements of the 1st series was 240mm while in the 2nd series was 110mm, see Fig. 4c. The following denotations were introduced: S - slab-column element without the concrete head, G - slab-column elements of the 1st series with drop panels, H - slab-column elements of the 2nd series with drop panels. The second part of the denotations is a number determining the number of the head dimension, while the third part is a number indicating the head dimension.

All slab-column elements were designed with C30/37 concrete class with a maximum aggregate size of 16mm, water-to-cement ratio of 0.55, and a content of 280 kg/m^3 portland cement CEM II 42.5R and 60kg/m^3 of fly ash. The concrete strength was determined on the day of testing of each element from the strength test of three cube specimens (150x150x150mm). The strength value obtained from tests on cube specimens was adjusted to cylindrical specimens using the formula recommended in the report published by FIB [56]: $f_{c,cyl} = 0{,}79 * f_{c,cube}$.

The concrete slabs were reinforced with an orthogonal mesh of 10mm diameter ribbed bars at 90mm spacing (8.73 cm^2/m), see Fig. 4c. The column was reinforced with eight 10mm diameter bars. The compression zone of the slab was not reinforced. The head compression zone of the 1st series elements was reinforced orthogonally with 8mm diameter bars at 120mm spacing in each direction. The compression zone of the head of the 2nd series elements was reinforced orthogonally with three 8mm diameter bars in each direction, see Fig. 4c. Reinforcing steel with a characteristic yield strength of f_{yk}=500MPa was used. The geometrical and mechanical properties of examined slab-column elements are given in Table 1. The reinforcement layout/ratio was chosen to avoid slab failure due to bending under punching tests.

Table 1. Geometrical and mechanical properties of examined elements.

Series no.		h_s	h_{sh}	$c_{sh,x} = c_{sh,y}$	d	ρ	$f_{c,\,cube}$	$f_{c,\,cyl}$

	Test element	[mm]	[mm]	[mm]	[mm]	[%]	[MPa]	[MPa]
1	S1-200	110	240	200	80	1.09	43.2	34.2
	G1-300	110	240	300	80	1.09	43.7	34.5
	G2-400	110	240	400	80	1.09	46.2	34.5
	G3-600	110	240	600	80	1.09	45.2	36.5
	G4-800	110	240	800	80	1.09	48.3	38.1
	G5-900	110	240	900	80	1.09	40.9	32.3
2	H3-600	110	110	600	80	1.09	39.3	31.0
	H4-800	110	110	800	80	1.09	39.3	31.0
	H5-900	110	110	900	80	1.09	30.4	24.0

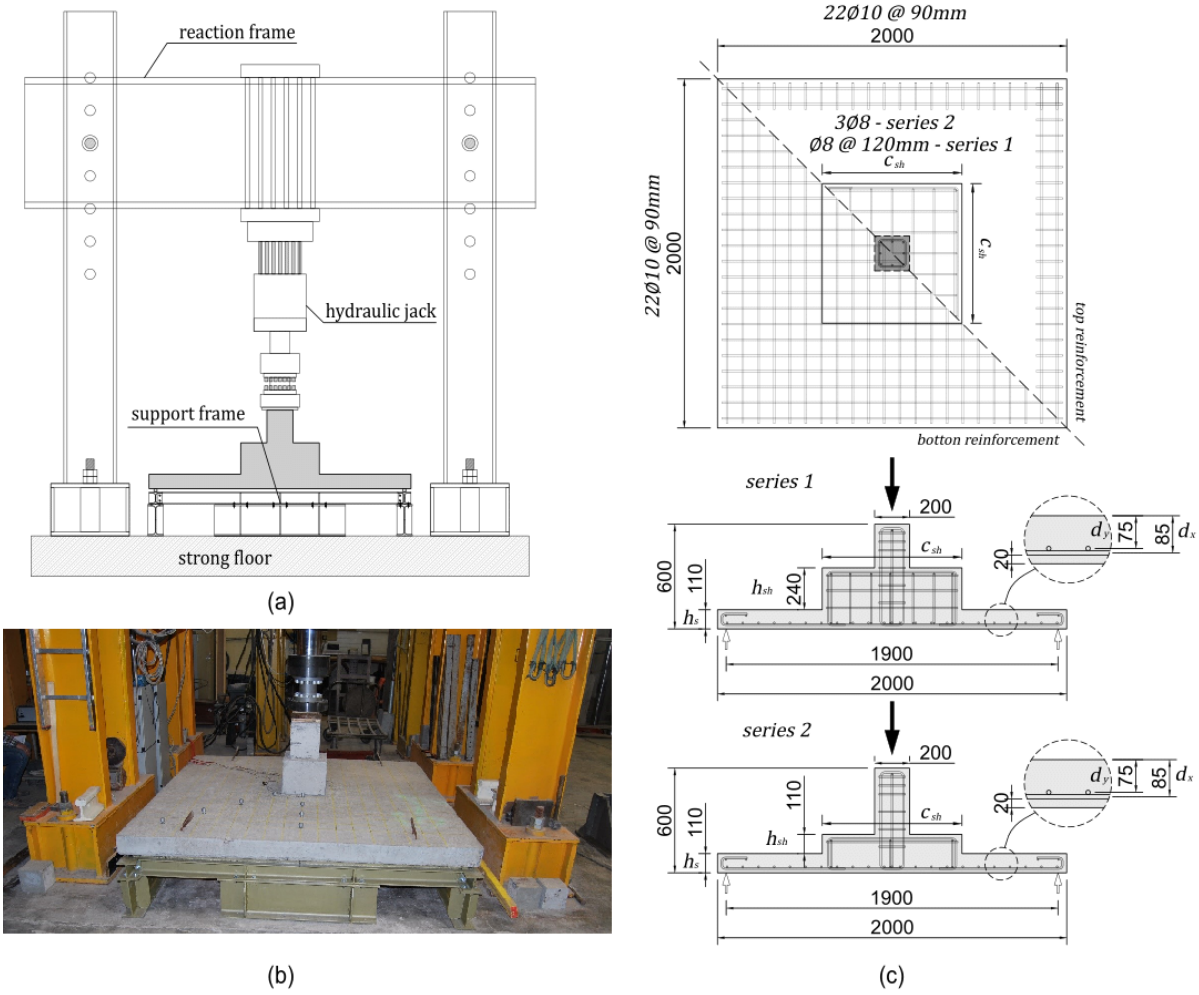

Fig. 4. Tested slab-column elements: (a) (b) Laboratory test stand, (c) dimensions and reinforcement

In the laboratory tests, the strength-testing computer-operated machine of Zwick type was applied. The hydraulic jack was computer-operated by the TextExpert program. The values of displacement and force on the hydraulic jack were recorded. All concrete slabs were subjected to vertical load with a force-controlled constant loading speed equal to 10 kN/s up to failure. The load was applied incrementally. All measurements were taken before the first load increment and after each subsequent load increment. The gap time between each increment was related to the measurement time and was taken as equal to 10 minutes. The hydraulic jack control parameters are shown in Table 2.

Table 2. Load control parameters.

Model	Speed of force development	Load increment	

			Gap between increments
	[kN/min]	[kN]	[min]
S1-200	10	20	10
G1-300	10	25	10
G2-400	10	35	10
G3-600	10	40	10
G4-800	10	50	10
G5-900	10	60	10
H3-600	10	40	10
H4-800	10	50	10
H5-900	10	60	10

2.3. Characteristics of measurement devices

The vertical displacement during the test was measured using dial indicators with an accuracy of 0.01mm. The laser distance measurer with an accuracy of 0.1mm was used as an additional measurement between the dial indicator values. Additionally, a terrestrial laser scanner (TLS) was used as a control measurement to measure the slab deformation, see Fig. 5. Based on spherical markers and scans of the whole element, the deformation of the plate at the moment of measurement was obtained, see Figs. 5 and 6. The classical point-to-point approach was used to calculate the deformation (see e.g. [57,58]). In this method, the individual areas are compared to a defined reference area, which expresses the state of the object before deformation (reference scan). By comparing the individual images (see Fig. 5), the slab displacement for each load increment was determined with an accuracy of 1mm. Measurements by terrestrial laser scanner of the 1st series of tests showed a correspondence of +/-2mm with the manual measurements.

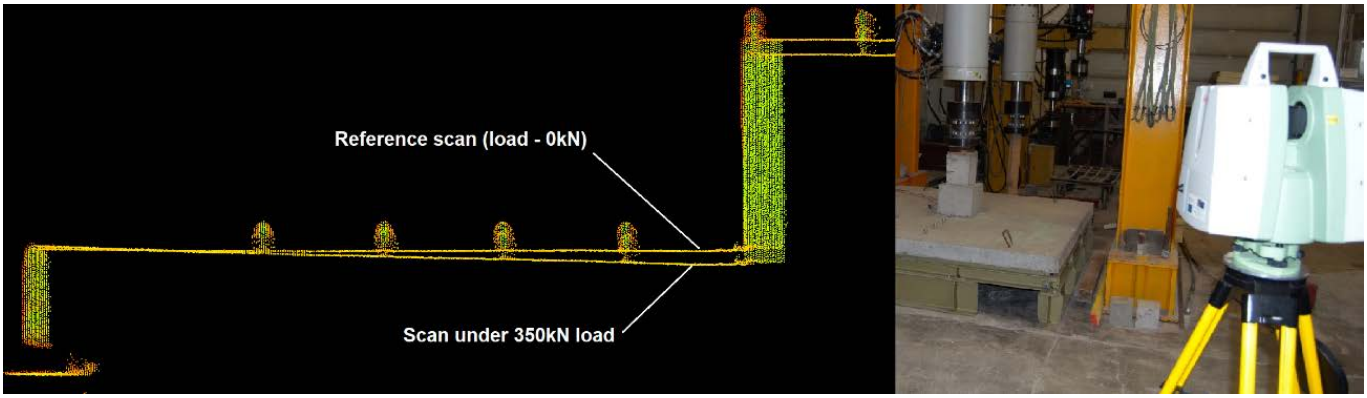

Fig. 5. TLS scans at 0 kN and 350 kN load for the G4-800 specimen.

Strains of the reinforcement were recorded using extensometers. Four extensometers were installed in each slab-column element (two extensometers per reinforcement direction). The extensometers were located in the cross-section of the outer head edge. One on the rebar passes centrally through the column. The other is located on the rebar passing near the edge of the head. The location of measuring points for the G3-600 and H3-600 test elements is shown in Figure 6.

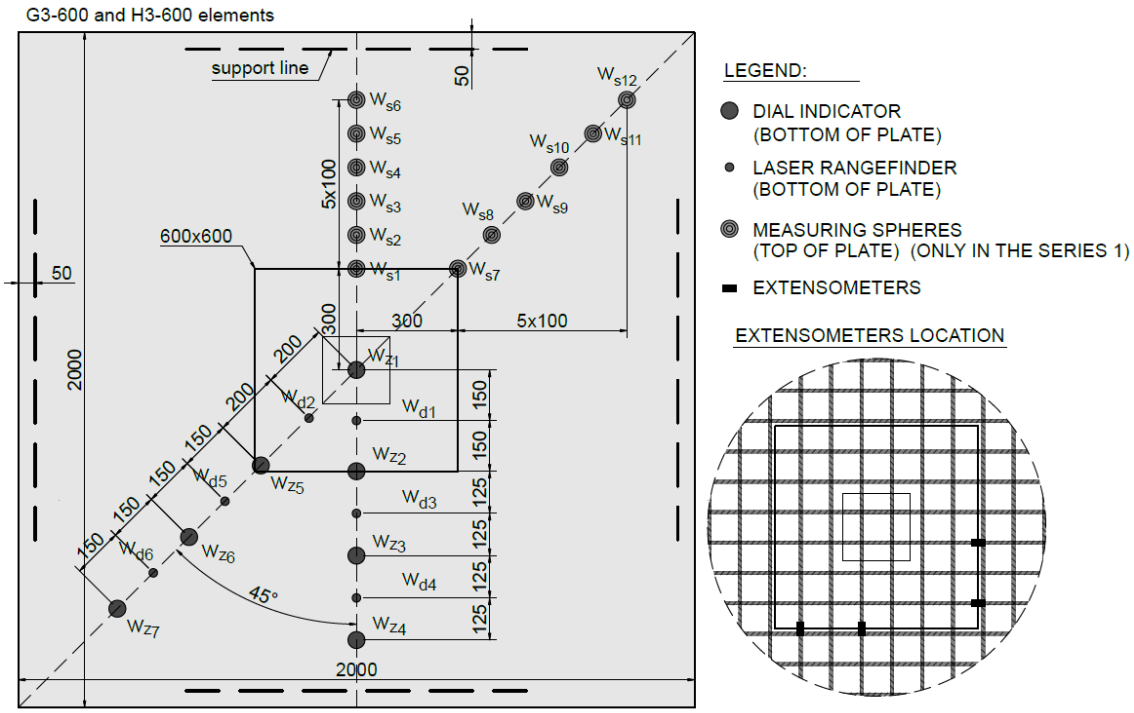

Fig. 6. Measuring points for G3-600 and H3-600 test elements.

All measurements of slab deformation were made after each increment of load. The measurements at the time of failure (due to the nature of the measuring method) were obtained by extrapolation from the obtained results. The value of the displacement at the moment of failure of the slab was calculated by extrapolating the last three (or four - depending on the development of the displacement-loading force relationship) measurements taken at a given point. The points were extrapolated by a second-degree polynomial, see Fig. 7.

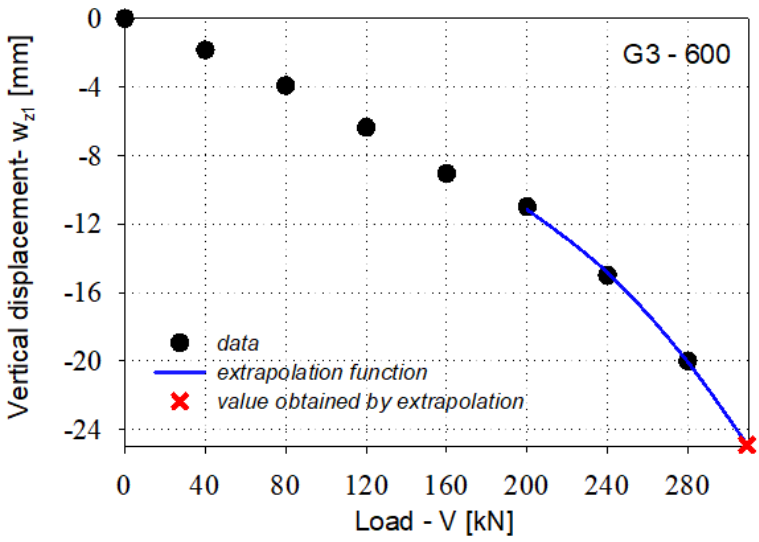

Fig. 7. Displacement extrapolation - element G3-600, measuring point w_{z1}.

3. *Laboratory test results*

3.1. Failure forces and form of failure.

Observation of the tested elements of the 1st series revealed the rapid nature of the failure for all slab elements. It was observed lost their punching shear resistance in the zone outside the drop panel. Two failure modes of slabs

were distinguished. In elements S1-200, G1-300, G2-400 and G3-600 the head (or column for element S1-200) penetrated the slab through the entire cross-section along the whole perimeter forming a characteristic cone. For elements G4-800 and G5-900, penetration through the entire cross-section of the slabs occurred only at the corners of the drop panel. The head also penetrated through the rest of its control perimeter. A clear vertical displacement of the entire head was observed. However, the tensile part of the plane of the slab remained continuous, see Fig. 8. The observed cracking process confirmed the observations known from previous studies. The first crack usually appeared parallel to the edge of the load field (head). Then, or simultaneously with the edge crack, radial cracks appeared extending from the corners of the heads to the support. The performed observations confirm the fact of generating concentrated internal forces near the corners of large-size rigid support (in this case a rigid drop panel). The failure mechanism of elements G4-800 and G5-900 suggests that these concentrations were the cause of failure. However, observation indicates a significant redistribution of shear forces as the entire compression zone of the control perimeter was 'sheared'. It can therefore be concluded that once the limiting shear force was obtained at the corners of the heads, the straight sections of the control perimeter were involved in the load transfer.

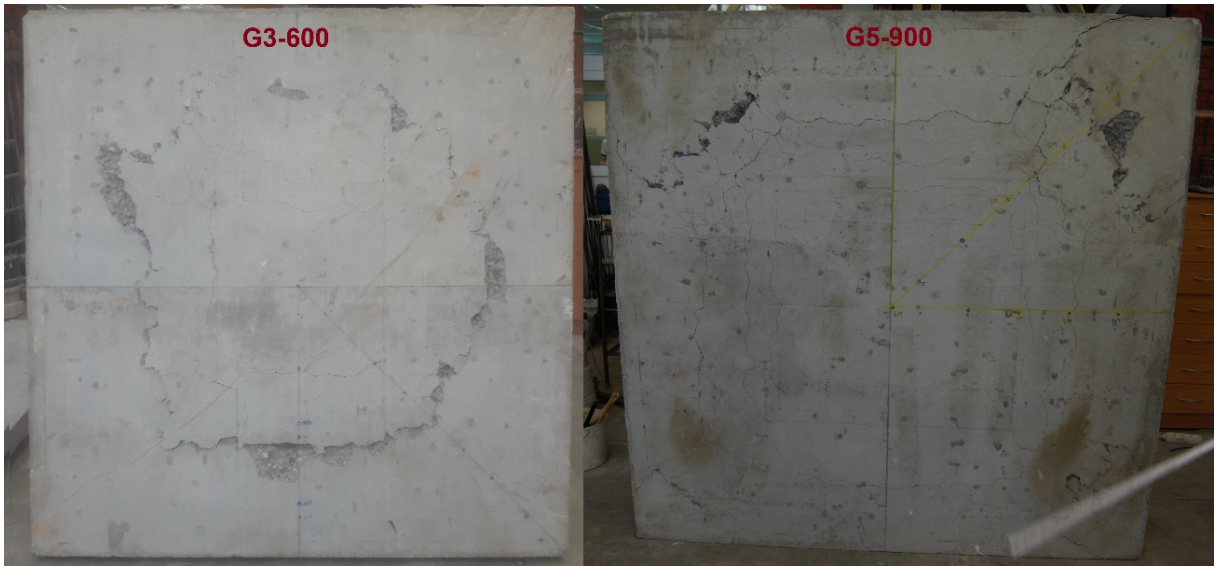

Fig. 8. Punching shear cracks: visible on the entire cross-section around the whole head (left), visible at the corners with straight segments of the control perimeter (right).

The elements of the 2nd test series were behave differently under loading. Element H3-600 failed by bending. Under large deformations of the reinforcing steel, the concrete of the compression zone of the slab and the head was crushed. Regions separated by yield lines were formed, see Fig. 9. In elements H4-800 and H5-900 a punching occurred inside the head, see Figs. 10 and 11. Significant deformation and cracking of the thickened part of the slab were observed during the test. The concrete of the head near the column was crushed at the moment of failure, see Figs. 10 and 11. The morphology of the cracking was different in comparison to the elements of the 1st series. The cracks mainly appeared parallel to the column near its edges and as radial cracks extending uniformly from the column loading surface to the support. The column heads were significantly deformed and revealed extensive cracking, see Fig. 12.

The 2nd series of tests clearly showed that the stiffness of the head is crucial to the failure mechanism and the load-bearing capacity of the test obtained. The flexible drop panels were not able to break through the slab. The application of the flexible head determined the failure mechanism by penetration inside the head or by bending, which resulted in a higher load capacity for H3-600 and H4-800 compared to the 1st series of tests (elements G3-600 and G4-800). Element H5-900 had a lower resistance than G5-900. However, it should be noted that the H5-900 element was made with a significantly lower concrete compressive than the other elements, see Table 1. With the reduction in capacity due to the strength of the concrete, elements G5-900 and H4-800 achieve very similar capacities to those obtained in the test of element H5-900, see Table 4.

Table 3. Failure forces specified under laboratory tests.

Specimen	V_R
	[kN]
S1-200	160
G1-300	238
G2-400	245
G3-600	310
G4-800	381
G5-900	420
H3-600	400
H4-800	391
H5-900	360

Table 4. Recalculation of the load capacity with adjustment to the compressive strength obtained for element H5-900.

Model	V_{exp}	$f_{c,\,cyl}$	$a_{red}=(f_{c,\,cyl,\,i})^{0.5} / (f_{c,\,cyl,\,H5})^{0.5}$	$V_{exp} * a_{red}$
	[kN]	[MPa]	[-]	[kN]
G5-900	420	32.3	0.86	362
H4-800	391	31.0	0.88	344
H5-900	360	24.0	1.00	360

Fig. 9. Failure form of H3-600 element.

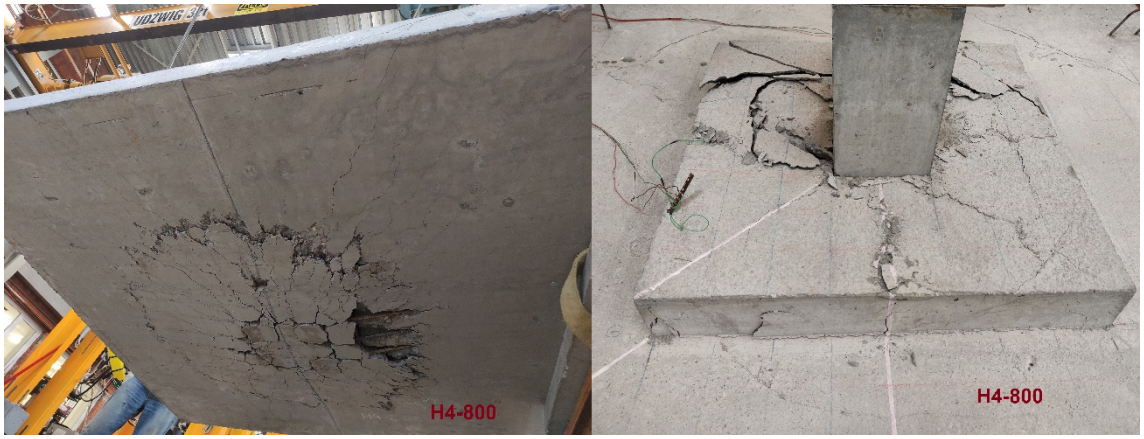

Fig. 10. Failure form of H4-800 element.

Fig. 11. Failure form of H5-900 element.

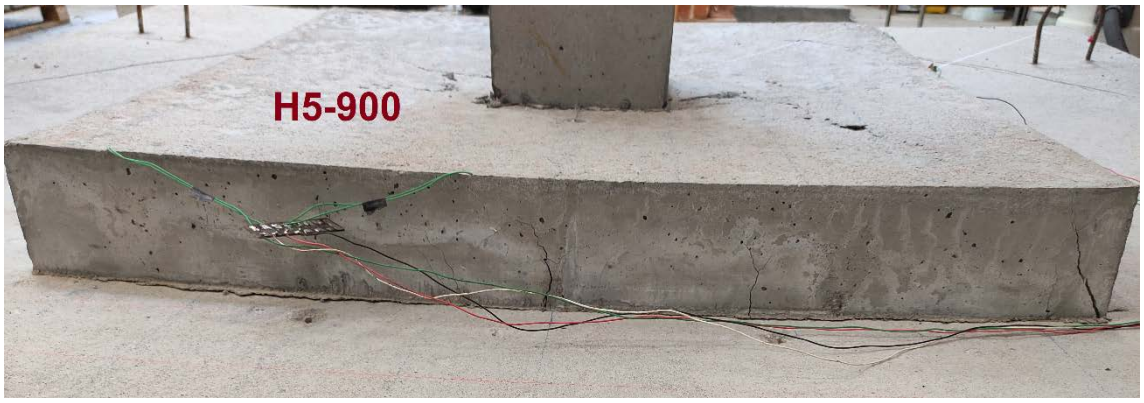

Fig. 12. H5-900 element with visible cracking on the head - load level ~ 95 - 100%.

3.2. Deformations of flexural reinforcement.

The measured strain of the reinforcing bars as a function of the load level is shown in Fig. 13. The yield point was reached at a relatively equal level of load ranging from 60 to 80% of the failure force for all elements. For elements G4-800, G5-900, H3-600 and H4-800, a greater variation in strain measurements in the range of up to 50% of the failure load can be observed. This may be due to the non-uniform distribution of internal forces in the initial phase of the loading. This non-uniformity of deformation of rebars in elements G4-800 and H3-600 retains practically to failure load, while in elements G5-900 and H4-800 these deformations become almost equal at approximately 75% of maximal load. Based

on the performed strain measurements it can be concluded that there was no clear difference between the reinforcement strains in the corner bars compared to the strains of the central bars.

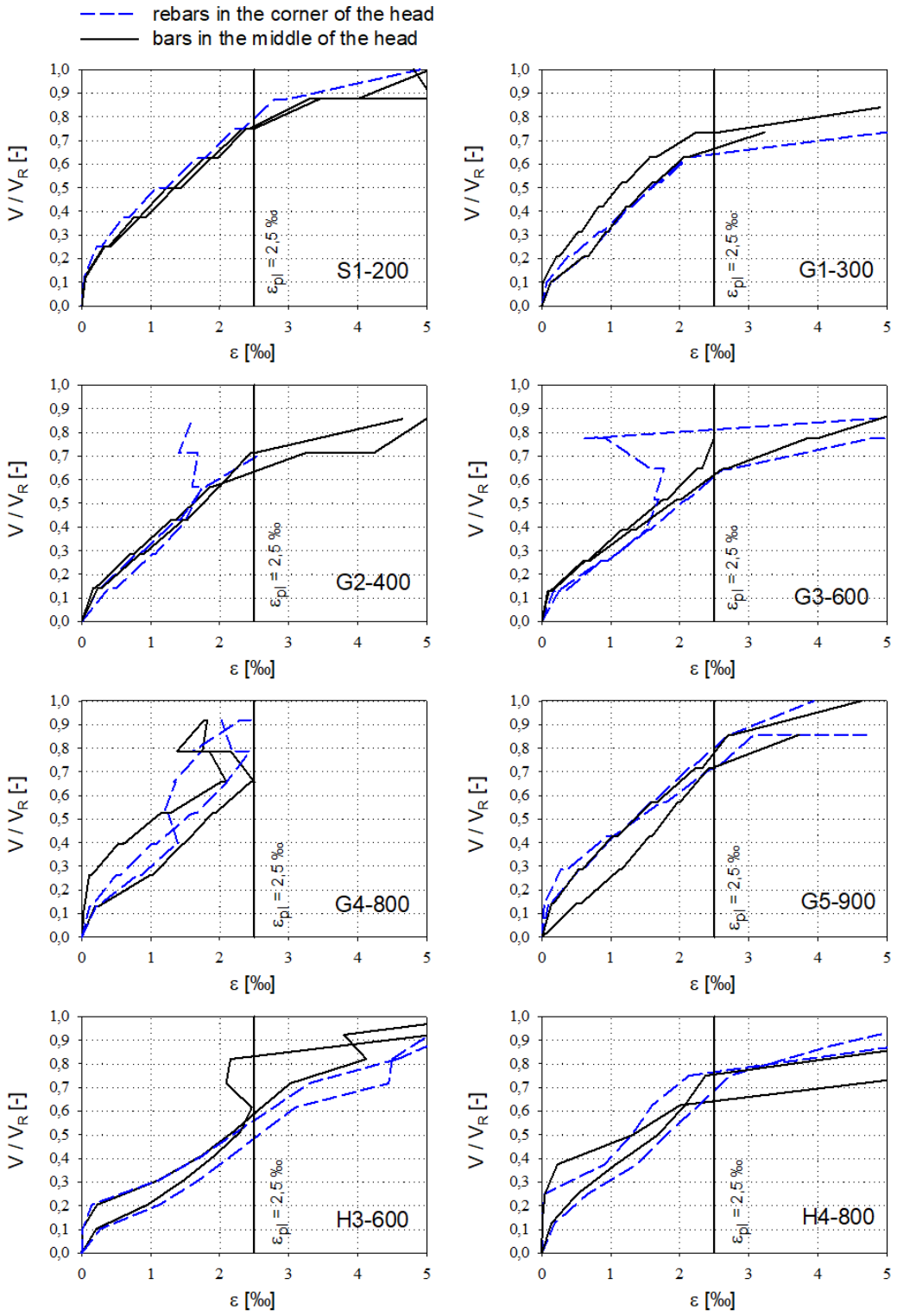

Fig. 13. The strain of reinforcing bars - strain gauge measurement.

3.2. Vertical displacement and rotation-load relationship.

Due to the high stiffness of the head, the measured displacement within the column and head of elements S1-200, G1-300, G2-400, and G3-600 were nearly the same. For the 2nd series test elements, the curvature within the head is greater due to the lower height of the head thickening. The deformation scheme of the tested elements and the

proposed method for calculating the head rotation angle (ψ_{sh}) and the plate rotation angle (ψ_s) is presented in Fig. 14. For the elements of the 1st series, only the rotation angles of the plate ψ_s were calculated (the rotation angle of the head ψ_{sh} was nearly equal to zero). For the elements of the 2nd series, a relation was derived for both the distinguished rotation angles. These relations were calculated from the vertical displacement measurements. The rotation angle in the line parallel to the edge of the plate ($\psi_{s,90}$ - calculated from the measurements from w_{z1} to w_{z4}) and in the diagonal of the plates ($\psi_{s,45}$ - calculated from the measurements from w_{z1} to w_{z7}) were distinguished. The force-rotation angle relationships of the slab-column elements are shown in Fig. 15. The dashed line indicates $V(\psi_{s,45})$ and the solid line $V(\psi_{s,90})$.

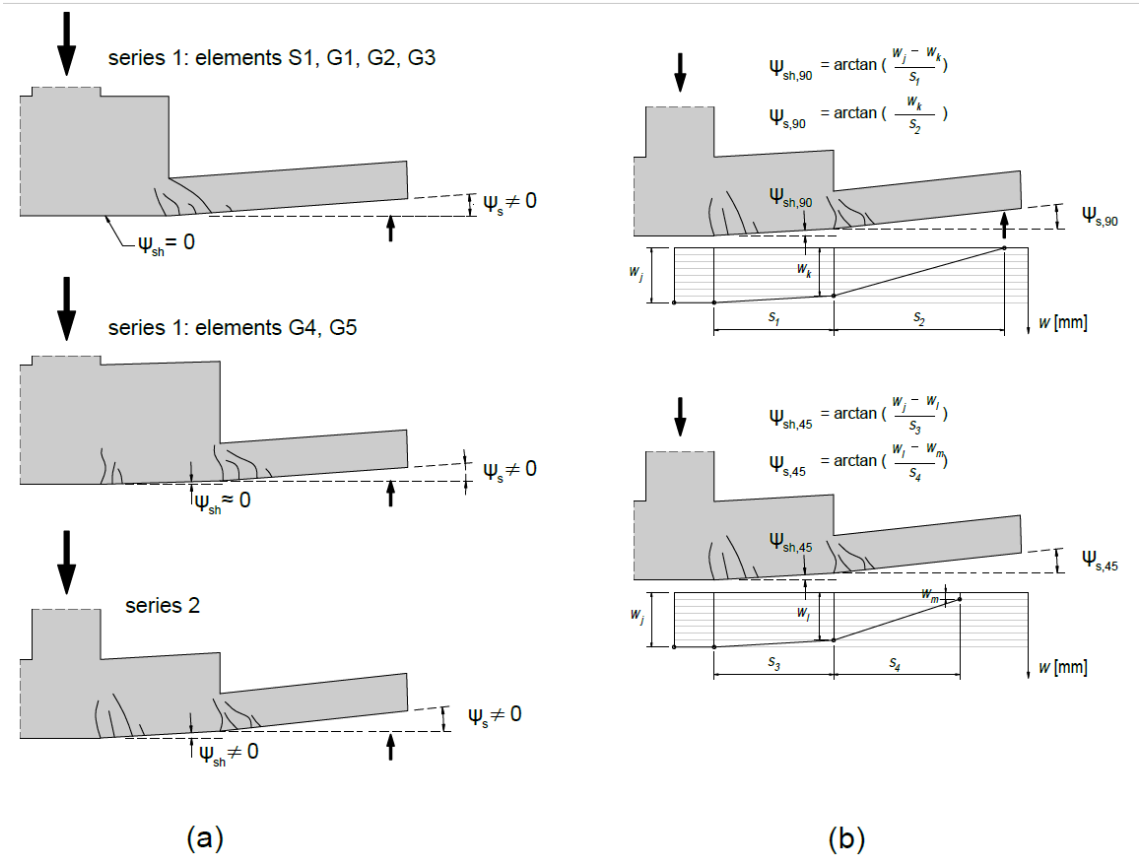

Fig. 14. Scheme of slab-column element deformation (a), Method for calculating the angle of rotation (b).

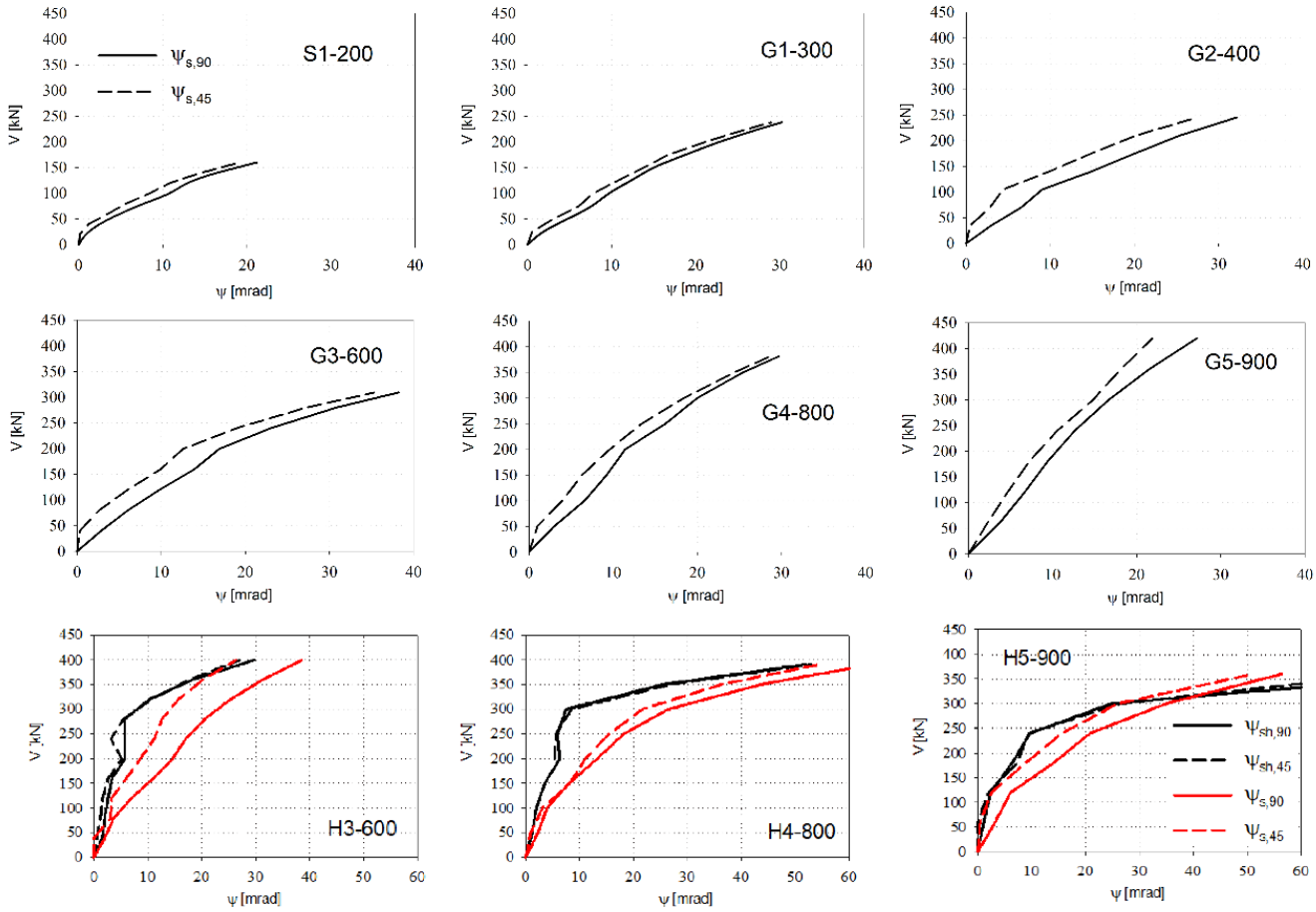

Fig. 15. Load-angle diagrams.

The angle of rotation on the diagonal of the element ($\psi_{s,45}$) was slightly smaller than the angle of rotation measured in the direction consistent with the distribution of reinforcement. The ultimate angle of rotation at failure increases with the drop panel dimension for specimens from S1-200 (c/d=2.5) to G3-600 (c/d = 7.5). Then the situation is reversed and for elements G4-800 (c/d=10) and G5-900 (c/d = 11.5), the ultimate angle of rotation is smaller. It can be concluded, that as the dimension of the support increased, more bars were within the geometry of the support and thus more reinforcement was directly used to transfer force from the loading jack to the supports. For example, it may be pointed out that four bars #10 in each direction (A_s=4*0.785= 3.1cm^2) pass through the head track of the G2-400 element, whereas ten bars #10 pass through the head track of the G5-900 element (A_s=10*0.785= 7.85cm^2). The smaller ultimate angle of rotation for the larger supports indicates a more rapid failure of models G4 and G5 compared to the other elements. The elements of the 2nd test series, due to lower head stiffness, showed different relationships compared to the corresponding elements of the 1st series (G3-600, G4-800, G5-900). The rotation angle of the head in elements H3-600 and H4-800 in the initial loading phase is much smaller than the rotation angle of the plate. This is due to the higher stiffness of the thicker head compared to the floor slab. After reaching approx. 70 - 75% of the failure force, the head shows significant cracking and its deformation increases, which ultimately leads to the failure of the elements at a comparable range of rotation angles of the slab and the head. The element that failed in bending (H3-600) at failure showed a ~19% smaller angle of rotation compared to the corresponding element of the first series (G3-600) - ~30mrad

/ ~37mrad = 0.81. Elements H4-800 and H5-900 (failure by puncture) showed significantly larger rotation angles at failure compared to elements G4-800 and G5-900 (H4/G4: ~52mrad / ~29mrad =1.79; H5/G5: ~80mrad / ~25mrad =3.20).

4. Discussion

4.1. Comparison of the experimental results with the theoretical calculations of the selected methods.

The punching resistance of the tested elements are compared to theoretical estimates following selected provisions: ACI318 [52], EC2 [59], EC2-DIN [51], MC2010 (LoA III) [53], CSCT [60]. Calculations for the CSCT method are presented for two variants of the control perimeter: a full control perimeter located at a distance of 0.5d from the head face (designation CSCT) and a reduced control perimeter to circular corners involving straight sections of length 3d (see figure 3c, designation CSCT-3d). Calculations by the CSCT theory were carried out based on the work of Guandalini [61]. The calculation script adapted the given method to the situation of a floor slab with a drop panel were created. The length of the control perimeter affects the failure criterion hence the difference in the theoretical load capacity obtained, see Fig. 16.

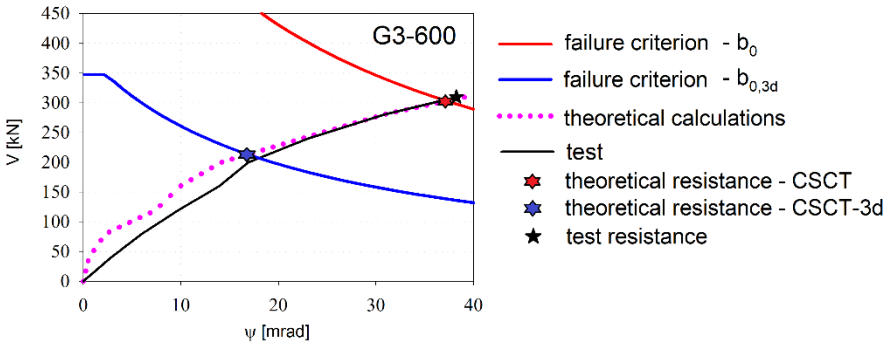

Fig. 16. Load capacity estimation using the CSCT method.

The calculations of the punching shear resistance according to the MC2010 standard were performed in four variants: for the full length of the control perimeter (designation MC2010), for the reduced control perimeter (MC2010-3d), for the control perimeter calculated according to the proposal of Vaz Rodrigues [54] (MC2010-Rod) and according to the proposal of Setiawan [55] (MC2010-Set), see Tables 5 and 6 and Fig. 17. Additionally, based on the yield line theory, the value of force at which failure of the plate occurs by bending was specified (designation V_{flex}). For investigated square elements supported close to the edges with the possibility of lift corners of the slab, loaded centrally, the V_{flex} was calculated as [62]

$$V_{flex} = \frac{8 \cdot m_{R,av}}{b_q} \cdot \left(0{,}5 \cdot c \cdot \left(\sqrt{2}-1\right)^2 + \left(\sqrt{2}-1\right) \cdot B\right), \tag{2}$$

where $m_{R,av}$ is the ultimate bending moment; b_q, c and B are the dimensions of the slab and support ($B = 2\,b_q + c$).

Calculations of the 2nd elements series were performed for the variant of punching inside the head and the variant of punching outside the drop panel.

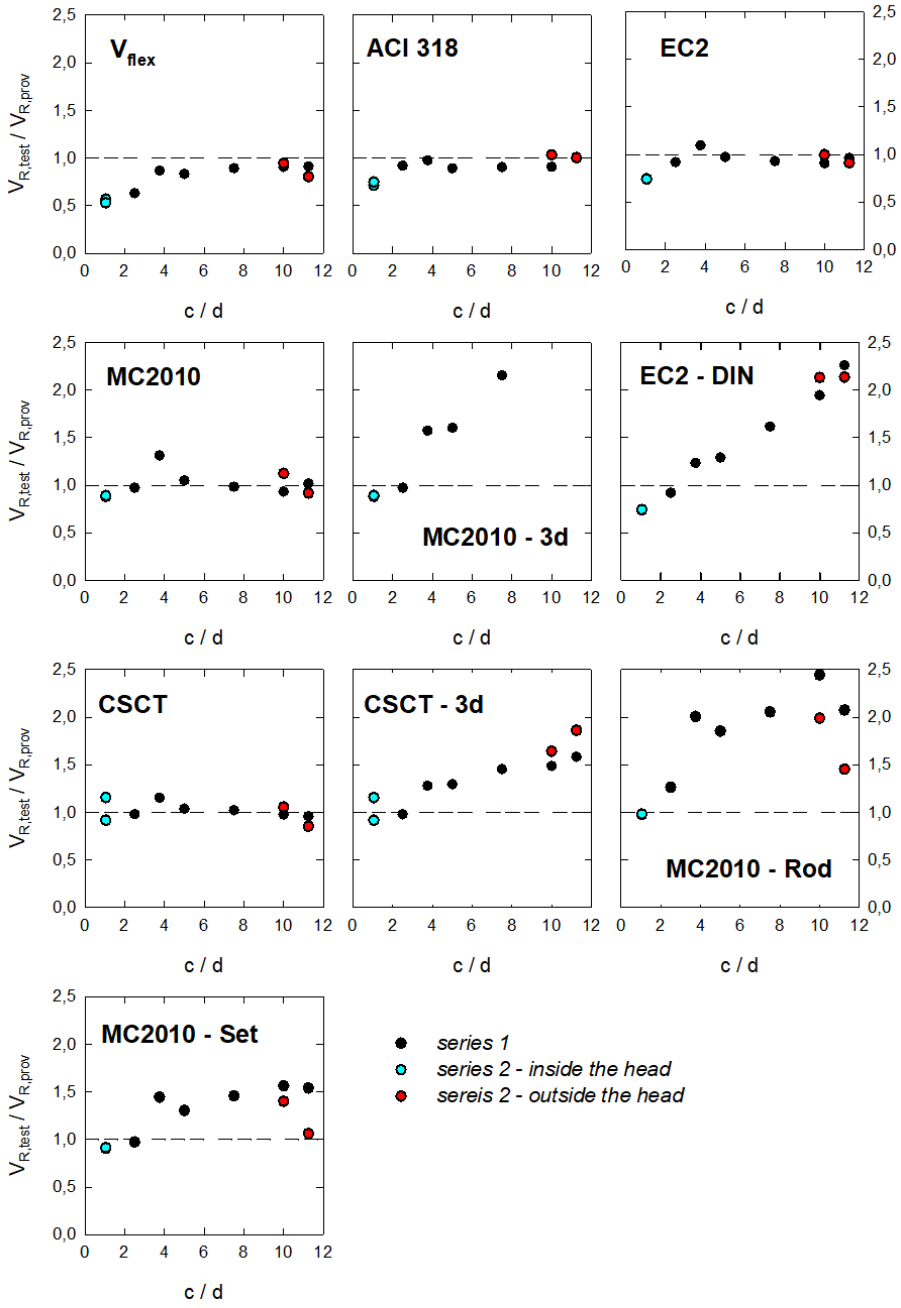

Fig. 17. Comparison of test results with calculations of selected methods.

Table 5. Comparison of actual failure forces with results of theoretical load capacity – 1st elements series.

Specimen	c / d	V_R	V_{flex}	V_{EC2}	$V_{EC2\text{-}DIN}$	V_{ACI}	V_{MC2010} (III LoA)	$V_{MC2010\text{-}3d}$ (III LoA)	$V_{MC2010\text{-}Rod}$ (III LoA)	$V_{MC2010\text{-}Set}$ (III LoA)	V_{CSCT}	$V_{CSCT\text{-}3d}$	V_R / V_{flex}	V_R / V_{EC2}	$V_R / V_{EC2\text{-}DIN}$	V_R / V_{ACI}	V_R / V_{MC2010}	$V_R / V_{MC2010\text{-}3d}$	$V_R / V_{MC2010\text{-}Rod}$	$V_R / V_{MC2010\text{-}Set}$	V_R / V_{CSCT}	$V_R / V_{CSCT\text{-}3d}$
	[-]	[kN]	[kN]	[kN]	[kN]	[kN]	[kN]	[kN]	[kN]	[kN]	[kN]	[kN]	[-]	[-]	[-]	[-]	[-]	[-]	[-]	[-]	[-]	[-]
S1-200	2,5	160	254	174	174	174	164	164	127	164	163	163	0.63	0.92	0.92	0.92	0.97	0.97	1.26	0.97	0.98	0.98
G1-300	3,75	238	274	217	193	244	181	151	119	165	206	186	0.87	1.10	1.23	0.98	1.31	1.57	2.01	1.45	1.16	1.28
G2-400	5	245	294	252	190	275	234	153	132	188	236	189	0.83	0.97	1.29	0.89	1.05	1.60	1.86	1.30	1.04	1.30
G3-600	7,5	310	347	333	192	343	315	144	151	213	303	213	0.89	0.93	1.61	0.90	0.98	2.15	2.06	1.46	1.02	1.46
G4-800	10	381	420	420	196	420	408	143	156	244	390	256	0.91	0.91	1.94	0.91	0.93	2.66	2.44	1.56	0.98	1.49
G5-900	11,3	420	462	435	186	416	413	130	202	273	438	265	0.91	0.97	2.26	1.01	1.02	3.23	2.08	1.54	0.96	1.58
												Average	0.84	0.97	1.54	0.93	1.04	2.03	1.95	1.38	1.02	1.42

Table 6. Comparison of actual failure forces with results of theoretical load capacity – 2nd elements series.

Specimen	c / d	V_R	V_{flex}	V_{EC2}	$V_{EC2\text{-}DIN}$	V_{ACI}	V_{MC2010} (III LoA)	$V_{MC2010\text{-}3d}$ (III LoA)	$V_{MC2010\text{-}Rod}$ (III LoA)	$V_{MC2010\text{-}Set}$ (III LoA)	V_{CSCT}	$V_{CSCT\text{-}3d}$	V_R / V_{flex}	V_R / V_{EC2}	$V_R / V_{EC2\text{-}DIN}$	V_R / V_{ACI}	V_R / V_{MC2010}	$V_R / V_{MC2010\text{-}3d}$	$V_R / V_{MC2010\text{-}Rod}$	$V_R / V_{MC2010\text{-}Set}$	V_R / V_{CSCT}	$V_R / V_{CSCT\text{-}3d}$
	[-]	[kN]	[kN]	[kN]	[kN]	[kN]	[kN]	[kN]	[kN]	[kN]	[kN]	[kN]	[-]	[-]	[-]	[-]	[-]	[-]	[-]	[-]	[-]	[-]
H3-600 in	1,05	400	344	-	-	-	-	-	-	-	-	-	-	-	-	-	-	-	-	-	-	-
H4-800 in	1,05	391	415	529	529	548	443	443	400	432	338	-	0.94	0.74	0.74	0.71	0.88	0.88	0.98	0.91	1.16	-
H5-900 in	1,05	360	448	485	485	482	405	405	367	394	392	-	0.80	0.74	0.74	0.75	0.89	0.89	0.98	0.91	0.92	-
H4-800 out	10	391	415	393	184	379	348	122	196	279	370	225	0.94	1.00	2.13	1.03	1.12	3.20	1.99	1.40	1.06	1.74
H5-900 out	11,3	360	448	395	169	359	393	124	247	339	421	226	0.80	0.91	2.14	1.00	0.92	2.91	1.46	1.06	0.86	1.59
												Average (in)	0.87	0.74	0.74	0.73	0.89	0.89	0.98	0.91	1.04	-
												Average (out)	0.87	0.95	2.13	1.02	1.02	3.06	1.72	1.23	0.96	1.67

„in” – punching inside the head

„out” – punching outside the head

4.2. Discussion of the 1st test series

The bending failure force calculations (V_{flex}) confirm that all 1st elements series failed due to punching. Calculation methods that do not take the reduction of the control perimeter into account (ACI318, EC2, MC2010 and CSCT) showed a very good representation of the punching load capacity. The largest overestimation of the punching load capacity is shown by ACI318. The average ratio of the experimental failure force to the calculated predicted failure force is 0.93, see Table 5. The ACI318 code method does not include the reinforcement ratio parameter in its procedures, and with a lower reinforcement ratio, the underestimation could be higher. The best representation of the experimental results is provided by the CSCT (average ratio $V_{R,test}$ / $V_{R,prov}$ equals 1.02). The MC2010 method is based on the CSCT method hence its results are very similar. The EC2 standard shows a marginally higher overestimation of bearing capacity compared to CSCT and MC2010. For EC2, the average $V_{R,test}$ / $V_{R,prov}$ ratio is 0.97. In this calculation method for all elements with $c/d > 4$, there is an underestimation of the load capacity.

Taking into account, according to the EC2, the allowable transverse stresses do not depend on the support size, it can be concluded that with increasing support size the increment of the connection resistance is smaller than the increment of the control perimeter length. All procedures containing a length reduction of the control perimeter show conservative results for the resistance calculation. In the control perimeter in the EC2-DIN and MC2010-3d, the resistance of straight sections of the slab in which one-way shear occurs is neglected. The consequence of this is that the ratio $V_{R,test}$ / $V_{R,prov}$ increases as the parameter c/d increases (for the larger support the larger section of the control perimeter is ignored in the calculation). In both methods, this increment is practically linear. In the case of the MC2010-3d method, the underestimation value is significantly higher than for the EC2-DIN method. Because the control perimeter according to MC2010 procedures is located at a distance of 0.5d from the edge compared to a distance of 2d adopted by the European standard. Therefore, the ratio of the length of the reduced control perimeter to the length of the entire perimeter in the MC2010 standard is greater. Considering the average value of the ratio of the failure force obtained from the experiment to the calculated failure force, the MC2010-Rod method is similar to the MC2010-3d method (ratios of 1.95 and 2.03). However, looking at the individual results it can be seen that for parameters c/d >5 the MC2010-Rod method gives more reasonable results. A better estimate of the load capacity is given by the MC2010-Set proposal. Similar results to MC2010-Set were obtained by performing CSCT-3d calculations. The large difference between the results of the MC2010-3d and CSCT-3d calculations is because, in the CSCT-3d method, the reduction of the control perimeter does not have a linear effect on the resistance of the connection.

The observation carried out during the laboratory tests confirms the fact that there are significant concentrations of internal forces at the corners of the thickening. On the other hand, the obtained load-bearing capacity results suggest that at the moment of failure the entire control perimeter was fully carrying the load. This testifies to the high possibility of redistribution of shear forces in this type of structure (c/d>4). The above analysis suggests that with such large supports, methods that reduce the length of the control perimeter do not succeed. It can be seen that in these methods,

when the support dimension is increased over c/d = 3, there is no increase in resistance, see Table 5. Therefore, a better solution seems to be to make the allowable transverse stresses in the connection depend on the support dimension.

4.3. Discussion of the 2nd test series

The drop panels of the 2nd test series elements were too flexible to lead to punching on the outside of the head, see Figure 17 and Table 6. Calculations by standard methods show that the weaker control perimeter where destruction should theoretically occur was the perimeter on the outside of the thickening. Only the CSCT calculations showed a minimally lower resistance in the control perimeter inside the drop panel, which was consistent with the actual behaviour of the plate. The ACI318 and EC2 standards (V_R / V_{prov} = 0.71-0.76) significantly overestimated the design punching resistance inside the drop panel. On the other hand, the calculation of the punching resistance in the control perimeter outside the head was a good estimate of the failure force. A similar situation occurs for the MC2010 calculations, except that the design punching resistance inside the head was slightly less overestimated (V_R / V_{prov} = 0.88-0.89). The observations of the test experiments and the calculations performed confirm a significant influence of the deformation (angle of rotation of the plate) on the load capacity of the joint. The higher deformation in the slab contributes to a lower punching resistance in the column-head joint. This is well illustrated by the CSCT calculation in which the deformation of the slab (its angle of rotation) is the key design parameter, see Fig. 18. The calculated load capacity of the H4-800 element (11cm slab + 24cm head in the 800x800mm range) is 338kN. The load capacity of the plate thickened to 24cm is 481kN.

In calculations with the CSCT method, if the whole slab is assumed in the head thickness, the punching resistance would be similarly overestimated as in the case of the other standard methods (V_R / V_{prov} = 391/481 = 0.80). It should be noted that this phenomenon occurs with flexible heads. Taking into account that the flexibility of the head can be determined by the ratio of the head height to its overhang beyond the edge of the column (h_{sh} / l_{sh}), it can be concluded that at a ratio $h_{sh}/l_{sh} \leq 0.55$ the heads are too flexible to cause punching outside the head, see Fig. 19.

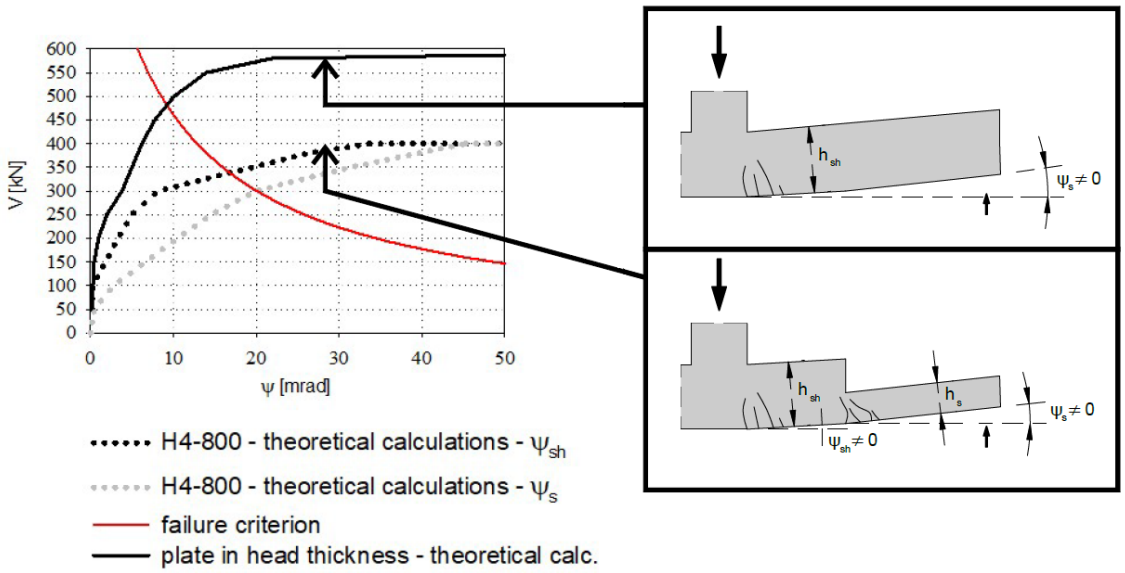

Fig. 18. Comparison of the behaviour of the element with and without drop panel according to CSCT calculations.

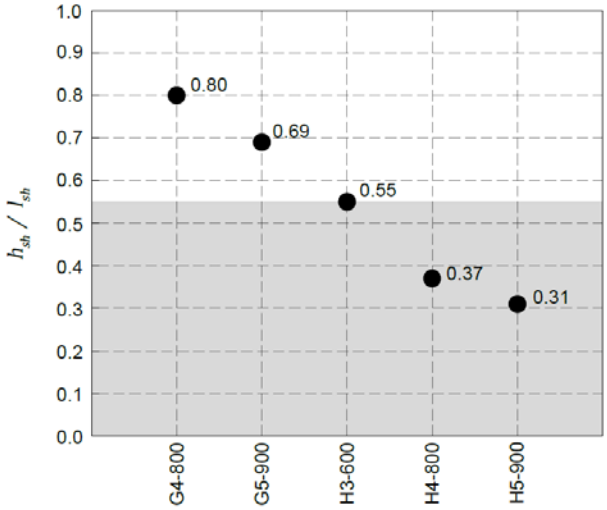

Fig. 19. Effect of head stiffness on failure mechanism.

4.2. Normalized transverse stresses in the control perimeter of the 1st test series.

Figure 20a shows the normalised shear stresses acting in the control section as a function of c/d for the results of the 1st series tests with available literature data collected in Table 7. The same test data were presented in Fig. 20b as a function of the failure force as a function of the support size (c_{max} / d). The failure force was divided by $\sqrt{f_c}$ and by *d* to exclude the influence of the concrete strength and the useful height of the slab on the results obtained. The graphs were made considering the control perimeter 0.5d away from the support with rounded corners. To compare the different studies, the authors adopted the criterion of the similar reinforcement ratio of the tested elements, since the flexural reinforcement significantly affects the allowable normalised shear stresses. Due to the low availability of experimental tests with large square supports, the reinforcement ratio criteria with rectangular support elements were also considered. It can be shown that as the support dimension increases, the allowable shear stress decreases. The decrease in allowable shear stress is evident in the range of the parameter c/d from 2.5 to 7.5. For the G3, G4 and G5 elements, the calculated allowable shear stresses remain relatively constant.

The results presented in Fig. 20b indicate that a load capacity increment is proportional to the support dimension in the range up to the value c_{max} =~4d. This is a less conservative result compared to what is assumed by the standard guidelines recommended a proportional increase of the load capacity to the support dimension c = 3*d* and then a reduction of this perimeter. The results also clearly show that for supports with dimension c >7d, straight sections (apart from corners extended by 2*d* on each side) provide an additional load-bearing capacity reserve which the standard guidelines recommended a reduction of the control perimeter do not take into account, see Fig. 21. The dark grey area represents the range of force that is transmitted through the control perimeter of the corners and straight sections of length 4*d*, while the light grey area is the force transmitted through straight sections of supports with a width greater than 7d. The experimental results confirm the significant contribution of one-way shear parts of the control perimeter to the total column-slab joint resistance for large support elements (c_{max} / d >7) [45].

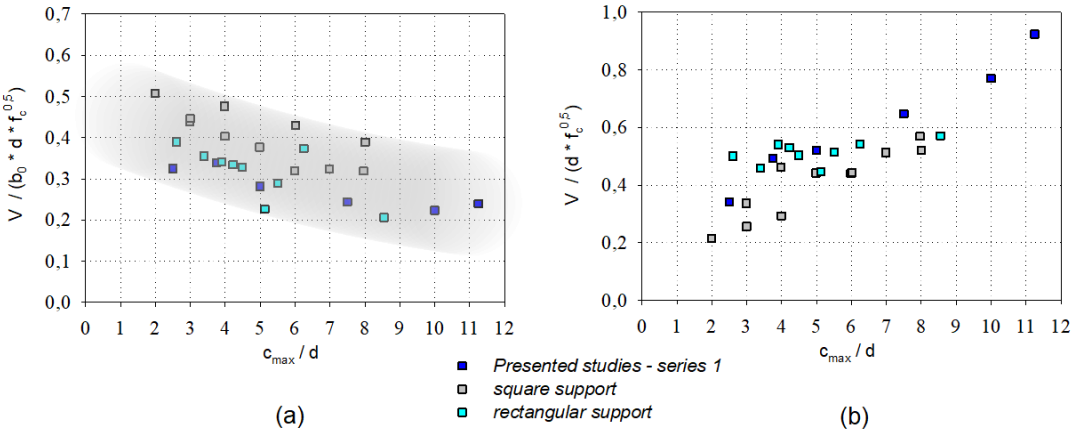

Fig. 20. (a) Ultimate shear stress depending on the parameter c_{max}/d; (b) Ultimate force depending on the parameter c_{max}/d.

Table 7. Chosen experimental data available for the column-slab connection.

Source	Specimen	Year	c_{max}	c_{min}	c_{max}/c_{min}	h	d	c_{max}/d	f_c	f_y	ρ_{lx}	ρ_{ly}	V_u
			[mm]	[mm]	[-]	[mm]	[mm]	[-]	[MPa]	[MPa]	[-]	[-]	[kN]
Present investigation	S1-200	2022	200	200	1	110	80	2.5	34.15	500	0.011	0.011	160
	G1-300	2022	300	300	1	110	80	3.8	36.53	500	0.011	0.011	238.3
	G2-400	2022	400	400	1	110	80	5.0	34.49	500	0.011	0.011	245
	G3-600	2022	600	600	1	110	80	7.5	35.7	500	0.011	0.011	309.5
	G4-800	2022	800	800	1	110	80	10.0	38.14	500	0.011	0.011	380.9
	G5-900	2022	900	900	1	110	80	11.3	32.28	500	0.011	0.011	420
Mowrer and Vanderbilt [63]	M-3-1-0	1967	152	152	1	76	51	3.0	21.1	386	0.011	0.011	79
	M-4-1-0	1967	203	203	1	76	51	4.0	15.5	386	0.011	0.011	93
	M-5-1-0	1967	254	254	1	76	51	5.0	23.3	386	0.011	0.011	109
	M-6-1-0	1967	305	305	1	76	51	6.0	28	386	0.011	0.011	119
	M-7-1-0	1967	356	356	1	76	51	7.0	27.8	386	0.011	0.011	138
	M-8-1-0	1967	406	406	1	76	51	8.0	24.9	386	0.011	0.011	145
Vanderbilt [42]	8S1-6	1972	305	305	1	51	38.1	8.0	20.5	295	0.010	0.010	90
	6S1-5	1972	229	229	1	51	38.1	6.0	21.2	296	0.010	0.010	78

	4S1-3	1972	152	152	1	51	38.1	4.0	20.8	296	0.010	0.010	51
	3S1-2	1972	114	114	1	51	38.1	3.0	23	303	0.010	0.010	47
	2S1-1	1972	76	76	1	51	38.1	2.0	27.6	303	0.010	0.010	43
Al.-Yousif and Regan [64]	2	2003	500	100	5	100	80	6.3	23.2	472	0.010	0.009	209
Teng et al. [65]	S13-090	2018	600	200	3	150	117	5.1	114	537	0.009	0.009	558
	S15-090	2018	1000	200	5	150	117	8.5	97	537	0.009	0.009	658
Oliveira et al. [12]	L3c	2004	360	120	3	130	106	3.4	54	750	0.011	0.011	358
	L4c	2004	480	120	4	130	107	4.5	56	750	0.011	0.011	404
	L5c	2004	600	120	5	130	109	5.5	63	750	0.011	0.011	446
Hawkins et al. [13]	7	1971	457	152	3.01	152	117.3	3.9	26.4	419	0.009	0.009	326
	8	1971	495	114	4.34	152	117.3	4.2	26.6	422	0.008	0.008	321
	9	1971	305	152	2.01	152	117.3	2.6	30.1	422	0.008	0.008	322

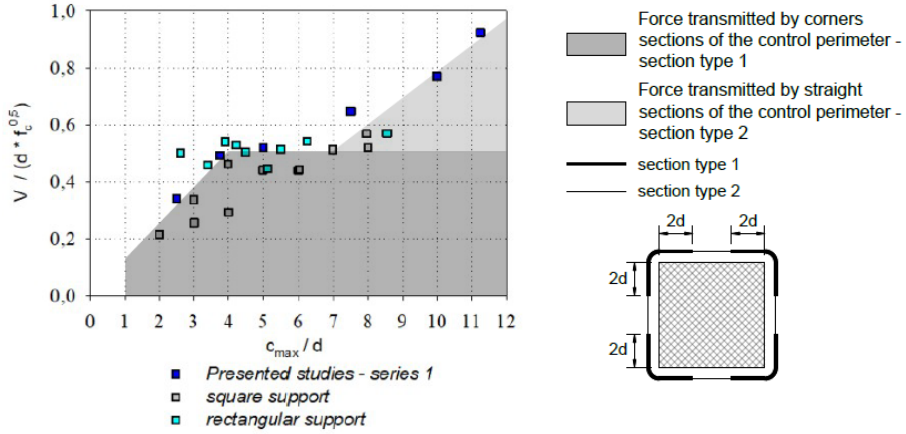

Fig. 21. Ultimate force depending on the parameter c_{max}/d. Interpretation of results.

4.2. Reduction factor of the support dimension on the punching resistance to the EC2.

The performed analysis shows that the allowable shear stresses at failure decrease with the increasing length of the testing control perimeter. The present EC2 standard [59] does not make the allowable shear stresses depend on the support dimension (all the test elements with c/d > 4 have an over-designed resistance). The analysis shows that the reduction of the control perimeter does not give design results compatible with the experimental tests (see Fig. 18, EC2-DIN). The authors propose an additional reduction factor k_{sh} that reduces the allowable transverse stresses in places of the control perimeter reduction, as follows:

$$v_{Rd,c} = C_{Rd,c} * k_{sh} * k * \sqrt[3]{100 * \rho_l * f_{ck}} + k_1 * \sigma_{cp} \quad (2)$$

where:

$$k_{sh} = \begin{cases} 1 & \rightarrow \quad c/d \leq 4 \\ 1 - 0.025 * (\frac{c}{d} - 4) & \rightarrow \quad 4 < c/d < 7 \\ 0.925 & \rightarrow \quad 7 > c/d \end{cases} \quad (3)$$

A comparison between the basic calculation of the EC2 standard and the proposed modification EC2+k_{sh} is given in Table 8. The proposed additional reduction factor results in a change in the average $V_{R,test}$ / $V_{R,prov}$ ratio from 0.96 to 1.01.

Table 8. The load punching capacity calculations of test elements by the EC2 and the proposed modification by the k_{sh} factor.

Test element	c	d	c/d	f_c	ρ_l	$v_{Rc,EC2}$	$b_{0,EC2}$	V_{EC2}	k_{sh}	$V_{EC2+ksh}$	V_R	V_R / V_{EC2}	$V_R / V_{EC2+ksh}$
	[cm]	[cm]	[-]	[MPa]	[-]	[MPa]	[cm]	[kN]	[-]	[kN]	[kN]	[-]	[-]
S1-200	20	8	2.5	34.2	0.011	1.21	180.5	174	1	174	160	0.92	0.92
G1-300	30	8	3.75	36.5	0.011	1.23	220.5	218	1	218	238	1.09	1.09
G2-400	40	8	5	34.5	0.011	1.21	260.5	252	0.975	246	245	0.97	1.00
G3-600	60	8	7.5	35.7	0.011	1.22	340.5	333	0.925	308	310	0.93	1.01
G4-800	80	8	10	38.1	0.011	1.25	420.5	421	0.925	389	381	0.91	0.98
G5-900	90	8	11.25	32.3	0.011	1.18	460.5	436	0.925	403	420	0.96	1.04
											mean	0.96	1.01

4. Conclusion.

This study presents unique experimental test results of the two series of slab-column elements topped with varying sizes of drop panels. The behaviour of the tested elements during the experimental test and the form of failure are described. Ultimate loads were compared with the selected calculation standards methods. The experimental test results were analysed in terms of allowable shear stresses. Based on performed experimental and analytical investigation the following conclusions may be drawn:

- The failure form of the tested slab-column elements depends on the stiffness of the drop panel. The elements of the 1st series (with rigid head) behaved as plates supported on a large column. The 2nd series of elements (with a flexible head) showed that it was not possible to reach the punching shear outside the drop panel due to insufficient stiffness. The stiffness of the head can be determined by the ratio of the head height to its extension beyond the edge of the column (h_{sh} / l_{sh}). The experimental test results show that at a ratio $h_{sh}/l_{sh} \leq 0.55$ the heads are too flexible to cause punching shear outside the head.
- Elements H4-800 and H5-900 were damaged by punching inside the drop panel. According to ACI318, EC2 and MC2010 (III LoA) standards, the failure should occur outside the drop panel. Thus, the ACI318 and EC2 standards overestimated the punching resistance inside the head by about 25%, while the MC2010 (IIILoA) standard overestimated the resistance to punching inside the head by about 10%. This result was due to the lower stiffness of the plates with partial thickening compared to the element with thickening over the entire range. This results in a larger rotation angle of the plate with partial thickening, leading to faster failure. The authors emphasise the need for more research on this type of connection.
- The 1st series of experimental tests confirm significant concentrations of shear forces at the corners of the large support. At the same time, they show a significant contribution of the rest of the control perimeter to the ultimate force transmitted by the slab-column joint.

- A comparative analysis of the chosen standard methods showed that all standard methods using the control perimeter length reduction approach due to the size of the support were far from the experimental results. The control perimeter reduction approach in the standard guidelines does not adequately fulfil its role. A better solution is the approach of reducing the allowable transverse stresses as a function of the support dimension by an additional reduction factor.

The obtained results encourage the authors to continue the research directed towards precisely understanding the influence of the drop panels size and stiffness on the behaviour of the connection between the flat slab and the column topped by the drop panel.

LITERATURE

[1] S. Garg, V. Agrawal, R. Nagar, Case study on strengthening methods for progressive collapse resistance of RC flat slab buildings, Structures. 29 (2021) 1709–1722. https://doi.org/10.1016/J.ISTRUC.2020.12.049.

[2] M. Buitrago, J. Sagaseta, J.M. Adam, Effects of sudden failure of shoring elements in concrete building structures under construction, Eng. Struct. 172 (2018) 508–522. https://doi.org/10.1016/J.ENGSTRUCT.2018.06.052.

[3] M. Buitrago, E. Bertolesi, J. Garzón-Roca, J. Sagaseta, J.M. Adam, A Parametric Computational Study of RC Building Structures under Corner-Column Removal Situations, Appl. Sci. 2020, Vol. 10, Page 8911. 10 (2020) 8911. https://doi.org/10.3390/APP10248911.

[4] J. Garzón-Roca, J. Sagaseta, M. Buitrago, J.M. Adam, Dynamic Punching Assessment of Edge Columns after Sudden Corner Column Removal, Struct. J. 118 (2021) 299–311. https://doi.org/10.14359/51728195.

[5] T. Yang, Z. Liu, J. Lian, Progressive collapse of RC flat slab substructures with unbonded posttensioning strands after the loss of an exterior column, Eng. Struct. 234 (2021) 111989. https://doi.org/10.1016/J.ENGSTRUCT.2021.111989.

[6] P. Schmidt, M. Kalus, J. Hegger, Critical view on the level of maximum punching strength of flat slabs and column bases using database evaluations, Struct. Concr. 22 (2021) 3646–3660. https://doi.org/10.1002/SUCO.202100374.

[7] A. Ambroziak, M. Grabski, On the methods of live loads application to slab-column structures, Mater. Bud. 1 (2019) 82–84. https://doi.org/10.15199/33.2019.01.15.

[8] A. Ambroziak, M. Grabski, Comparison of punching shear calculation methods, Mater. Bud. 563 (2019) 52–55. https://doi.org/10.15199/33.2019.07.08.

[9] J. Halvoník, A. Vidaković, V. Borzovič, Failure analysis of collapsed parking garage building due to punching, Eng. Fail. Anal. 129 (2021) 105712. https://doi.org/10.1016/j.engfailanal.2021.105712.

[10] S. King, N.J. Delatte, Collapse of 2000 Commonwealth Avenue: Punching Shear Case Study, J. Perform. Constr. Facil. 18 (2004) 54–61. https://doi.org/10.1061/(ASCE)0887-3828(2004)18:1(54).

[11] J. Sagaseta, L. Tassinari, M. Fernández Ruiz, A. Muttoni, Punching of flat slabs supported on rectangular columns, Eng. Struct. 77 (2014) 17–33. https://doi.org/10.1016/j.engstruct.2014.07.007.

[12] D.R.C. Oliveira, P.E. Regan, G.S.S.A. Melo, Punching resistance of RC slabs with rectangular columns, Mag. Concr. Res. 56 (2004) 123–138. https://doi.org/10.1680/macr.2004.56.3.123.

[13] N.M. Hawkins, H.B. Fallsen, R.C. Hinojosa, Influence of column rectangularity on the behavior of flat plate structures, ACI J. Proc. 69 (1972) 127–146.

[14] H. Marzouk, A. Hussein, Experimental investigation on the behavior of high-strength concrete slabs, ACI Struct. J. 88 (1991) 701–713. https://doi.org/10.14359/1261.

[15] M.M.G. Inácio, A.F.O. Almeida, D.M.V. Faria, V.J.G. Lúcio, A.P. Ramos, Punching of high strength concrete flat slabs without shear reinforcement, Eng. Struct. 103 (2015) 275–284. https://doi.org/10.1016/J.ENGSTRUCT.2015.09.010.

[16] M.M.G. Inácio, M. Lapi, A. Pinho Ramos, Punching of reinforced concrete flat slabs – Rational use of high strength concrete, Eng. Struct. 206 (2020) 110194. https://doi.org/10.1016/J.ENGSTRUCT.2020.110194.

[17] T. Urban, M. Gołdyn, How To Strengthen Flat Slabs on Punching Shear – Traditionally With Steel or Innovative, By Using Fiber Composite Materials?, Eng. Struct. Technol. 11 (2019) 57–65. https://doi.org/10.3846/est.2019.10657.

[18] T. Urban, M. Gołdyn, Ł. Krawczyk, Ł. Sowa, Experimental investigations on punching shear of lightweight aggregate concrete flat slabs, Eng. Struct. 197 (2019) 109371. https://doi.org/10.1016/j.engstruct.2019.109371.

[19] S. Teng, H.K. Cheong, K.L. Kuang, J.Z. Geng, Punching Shear Strength of Slabs with Openings and Supported on Rectangular Columns, Struct. J. 101 (2004) 678–687.

[20] M. Gołdyn, T. Urban, The effect of openings size and location on the punching shear carrying capacity of the support zones of flat slabs in the light of the existing experimental investigations, Inżynieria i Bud. 75 (2019) 165–170.

[21] B. Belletti, J.C. Walraven, F. Trapani, Evaluation of compressive membrane action effects on punching shear resistance of reinforced concrete slabs, Eng. Struct. 95 (2015) 25–39. https://doi.org/10.1016/j.engstruct.2015.03.043.

[22] J. Einpaul, M. Fernández Ruiz, A. Muttoni, Influence of moment redistribution and compressive membrane action on punching strength of flat slabs, Eng. Struct. 86 (2015) 43–57. https://doi.org/10.1016/j.engstruct.2014.12.032.

[23] A.F.O. Almeida, M.M.G. Inácio, V.J.G. Lúcio, A.P. Ramos, Punching behaviour of RC flat slabs under reversed horizontal cyclic loading, Eng. Struct. 117 (2016) 204–219. https://doi.org/10.1016/j.engstruct.2016.03.007.

[24] I. Robertson, G. Johnson, Cyclic lateral loading of nonductile slab-column connections, ACI Struct. J. 103 (2006) 356–364. https://doi.org/10.14359/15313.

[25] B. Wieczorek, Wewnętrzna strefa podporowa żelbetowego ustroju płytowo-słupowego w stanie awaryjnym wywołanym przebiciem płyty, Wydawnictwo Politechniki Śląskiej, Gliwice, Poland, 2019.

[26] M. Diao, Y. Li, H. Guan, X. Lu, H. Xue, Z. Hao, Post-punching mechanisms of slab–column joints under upward and downward punching actions, Mag. Concr. Res. 73 (2021) 302–314. https://doi.org/10.1680/jmacr.19.00217.

[27] A. Pinho Ramos, V.J.G. Lúcio, Post-punching behaviour of prestressed concrete flat slabs, Mag. Concr. Res. 60 (2008) 245–251. https://doi.org/10.1680/macr.2008.60.4.245.

[28] B. Wieczorek, Influence of the location of the column on the load capacity of a slab-column connection for the inner column after punching, Procedia Eng. 57 (2013) 1251–1259. https://doi.org/10.1016/j.proeng.2013.04.158.

[29] M.F. Ruiz, A. Muttoni, J. Kunz, Strengthening of flat slabs against punching shear using post-installed shear reinforcement, ACI Struct. J. 107 (2010) 434–442. https://doi.org/10.14359/51663816.

[30] S. Guandalini, O.L. Burdet, A. Muttoni, Punching tests of slabs with low reinforcement ratios, ACI Struct. J. 106 (2009) 87–95. https://doi.org/10.14359/56287.

[31] S. Lips, Punching of flat slabs with large amounts of shear reinforcement, PhD Thesis, École Polytechnique Fédérale de Lausanne, Suisse, 2012. https://doi.org/10.1056/NEJMoa1208799.

[32] P. Schmidt, D. Kueres, J. Hegger, Punching shear behavior of reinforced concrete flat slabs with a varying amount of shear reinforcement, Struct. Concr. 21 (2020) 235–246. https://doi.org/10.1002/suco.201900017.

[33] B. Wieczorek, W. Starosolski, Wpływ mimośrodu obciążenia na nośność połączenia płyta-słup po przebiciu, Zesz. Nauk. Politech. Rzesz. Bud. i Inżynieria Środowiska. 59 (2012) 133–140.

[34] P.M. Lewiński, P.P. Więch, Finite element model and test results for punching shear failure of RC slabs, Arch. Civ. Mech. Eng. 20 (2020) 1–16. https://doi.org/10.1007/s43452-020-00037-x.

[35] M.H. Oliveira, M.J.M. Pereira Filho, D.R.C. Oliveira, M.P. Ferreira, G.S.S.A. Melo, M. Br, Punching resistance of internal slab-column connections with double-headed shear studs, Rev. IBRACON Estruturas e Mater. 6 (2013) 681–714. https://doi.org/10.1590/S1983-41952013000500002.

[36] D. V. Bompa, A.Y. Elghazouli, Structural performance of RC flat slabs connected to steel columns with shear heads, Eng. Struct. 117 (2016) 161–183. https://doi.org/10.1016/j.engstruct.2016.03.022.

[37] D. V. Bompa, A.Y. Elghazouli, Numerical modelling and parametric assessment of hybrid flat slabs with steel shear heads, Eng. Struct. 142 (2017) 67–83. https://doi.org/10.1016/j.engstruct.2017.03.070.

[38] M. Gołdyn, T. Urban, UHPFRC hidden capitals as an alternative method for increasing punching shear resistance of LWAC flat slabs, Eng. Struct. 271 (2022) 114906. https://doi.org/10.1016/j.engstruct.2022.114906.

[39] M. Gołdyn, T. Urban, Hidden capital as an alternative method for increasing punching shear resistance of LWCA flat slabs, Arch. Civ. Eng. Vol. 65 (2019) 309–328.

[40] M. Grabski, Punching shear capacity in the connection of the slab to column topped with a head, Gdansk University of Technology, 2022.

[41] M. Grabski, A. Ambroziak, Shear cap size selection method based on parametric analysis of ACI-318 code and eurocode 2 standard, Materials (Basel). 13 (2020) 1–24. https://doi.org/10.3390/ma13214938.

[42] M.D. Vanderbilt, Shear Strength of Continuous Plates, J. Struct. Div. 98 (1972) 961–973.

[43] T. Urban, Nośność na przebicie w aspekcie proporcji boków słupa. Badania doświadczalne elementów i konstrukcji betonowych. Raport 3., Łódź, 1994.

[44] G.J. Milligan, M.A. Polak, C. Zurell, Finite element analysis of punching shear behaviour of concrete slabs supported on rectangular columns, Eng. Struct. 224 (2020) 111189. https://doi.org/10.1016/J.ENGSTRUCT.2020.111189.

[45] M. Grabski, A. Ambroziak, Influence of the shear cap size and stiffness on the distribution of shear forces in flat slabs, Materials (Basel). 15 (2022). https://doi.org/10.3390/MA15010188.

[46] A. Setiawan, R.L. Vollum, L. Macorini, B.A. Izzuddin, Punching of RC slabs without transverse reinforcement

supported on elongated columns, Structures. 27 (2020) 2048–2068. https://doi.org/10.1016/J.ISTRUC.2020.08.017.

[47] J. Sagaseta, A. Muttoni, M.F. Ruiz, L. Tassinari, Non-axis-symmetrical punching shear around internal columns of RC slabs without transverse reinforcement, Mag. Concr. Res. 63 (2011) 441–457. https://doi.org/10.1680/macr.10.00098.

[48] J. Einpaul, J. Bujnak, M.F. Ruiz, A. Muttoni, Study on influence of column size and slab slenderness on punching strength, ACI Struct. J. 113 (2016) 135–146. https://doi.org/10.14359/51687945.

[49] G.J. Milligan, M. Anna Polak, C. Zurell, Impact of Column Rectangularity on Punching Shear Strength: Code Predictions versus Finite Element Analysis, J. Struct. Eng. 147 (2021) 04020331. https://doi.org/10.1061/(asce)st.1943-541x.0002889.

[50] CEN (European Committee for Standardization), EN 1992-1-1 Eurocode 2: Design of concrete structures - Part 1-1: General rules and rules for buildings., CEN (European Committee for Standardization), Brussels, Belgium, 2004.

[51] DIBt (Deutsche Institut für Bautechnik), DIN EN 1992-1-1/NA:2011-01 Nationaler Anhand – National festgelegte Parameter – Eurocode 2: Bemessung und Konstruktion von Stahlbeton und Spannbetontragwerken. Teil 1-1: Allgemeine Bemessungsregeln und Regeln für den Hochbau., 2011.

[52] ACI (American Concrete Institute), ACI 318-14 Building Code Requirements for Structural Concrete, (2014).

[53] FIB (International Federation for Structural Concrete), fib Model Code for Concrete Structures 2010, Ernst & Sohn, 2013.

[54] R. Vaz Rodrigues, M. Fernández Ruiz, A. Muttoni, Shear strength of R/C bridge cantilever slabs, Eng. Struct. 30 (2008) 3024–3033. https://doi.org/10.1016/j.engstruct.2008.04.017.

[55] A. Setiawan, R.L. Vollum, L. Macorini, B.A. Izzuddin, Punching shear design of RC flat slabs supported on wall corners, Struct. Concr. 21 (2020) 859–874. https://doi.org/10.1002/suco.201900514.

[56] K.-H. Reineck, R. Beutel, H. Duda, D. Goossens, M. Hallgren, D. Kuchma, S. McCabe, P. Menétrey, J. Niwa, J. Ozbolt, M.A. Pollak, A. Sherif, M. Staller, H. Vocke, fib Bulletin 12. Punching of structural concrete slabs, fib. The International Federation for Structural Concrete, 2001. https://doi.org/10.35789/fib.BULL.0012.

[57] P. Ziolkowski, J. Szulwic, M. Miskiewicz, Deformation Analysis of a Composite Bridge during Proof Loading Using Point Cloud Processing, Sensors. 18 (2018) 4332. https://doi.org/10.3390/s18124332.

[58] A. Janowski, K. Nagrodzka-Godycka, J. Szulwic, P. Ziolkowski, Remote sensing and photogrammetry techniques in diagnostics of concrete structures, Comput. Concr. 18 (2016) 405–420. https://doi.org/10.12989/cac.2016.18.3.405.

[59] PN-EN 1992-1-1: 2008/NA:2010 Eurokod 2: Projektowanie konstrukcji z betonu. Część 1-1: Reguły ogólne dla budynków., n.d.

[60] A. Muttoni, Punching shear strength of reinforced concrete slabs without transverse reinforcement, ACI Struct. J. 105 (2008) 440–450.

[61] S. Guandalini, Poinçonnement symétrique des dalles en béton armé., EPFL, 2005.

[62] J. Einpaul, Punching strength of continuous flat slabs, Lausanne, EPFL, 2017. https://doi.org/10.5075/epfl-thesis-6928.

[63] R.D. Mowrer, M.D. Vanderbilt, Shear Strength of Lightweight Aggregate Reinforced Concrete Flat Plates, J. Proc. 64 (1967) 722–729.

[64] A.T. Al-Yousif, P.E. Regan, Punching resistances of rc slabs supported by large and/or elongated columns, Struct. Eng. 81 (2003) 30–34.

[65] S. Teng, K. Chanthabouala, D.T.Y. Lim, R. Hidayat, Punching Shear Strength of Slabs and Influence of Low Reinforcement Ratio, ACI Struct. J. 115 (2018) 139–150. https://doi.org/10.14359/51701089.